Supplementary Information

Z-Scheme Charge Transfer between Conjugated Polymer and α-Fe_2O_3 for Simultaneous Photocatalytic H_2 Evolution and Ofloxacin Degradation

Ziheng Xiao[a], Jie Xiao[a], Luxi Yuan[a], Minhua Ai[a,b]*, Faryal Idrees[c], Zhen-Feng Huang[a,b,d], Chengxiang Shi[a,b,d], Xiangwen Zhang[a,b,d], Lun Pan[a,b,d], Ji-Jun Zou[a,b,c]*

[a] Key Laboratory for Green Chemical Technology of the Ministry of Education, School of Chemical Engineering and Technology, Tianjin University, Tianjin 300072, China.

[b] Collaborative Innovative Center of Chemical Science and Engineering (Tianjin), Tianjin 300072, China.

[c] Department of Physics, University of the Punjab, Quaid-e-Azam Campus, Lahore 54590, Pakistan.

[d] Haihe Laboratory of Sustainable Chemical Transformations, Tianjin 300192, China.

* Corresponding author.

E-mail: aiminhua@tju.edu.cn (M. Ai), jj_zou@tju.edu.cn (J.-J. Zou).

1. Materials

p-Diethynylbenzene (PEB, 97%) was purchased from Energy Chemical (Shanghai, China). bis(triphenylphosphine)palladium (II) dichloride ($Pd(PPh_3)_2Cl_2$, 98%) and Cuprous Iodide (CuI, 98%) were purchased from Heowns Biochemical Technology Co., Ltd. (Tianjin, China). N,N-dimethylformamide (DMF, GR), trimethylamine (TEA, GR), were obtained from Kermel Chemical Reagent Co., Ltd (Tianjin, China). 3,7-dibromodibenzo[b,d]thiophene 5,5-dioxide was prepared based on reported methods.[1]

Potassium ferrate (K_2FeO_4, 95%, black powder) was purchased from Maya Reagent Co., Ltd (Jiaxing, China). Methylene Blue (MB, AR), Triethanolamine (TEOA, 99%) was purchased from Aladdin Biochemical Technology Co., Ltd (Shanghai, China). Ofloxacin (OFL, 98%) was purchased from McLean Reagent Co., Ltd (Shanghai, China). High-purity water is self-made in the laboratory, and the conductivity is not lower than 18 MΩ·cm.

2. Characterizations

X-ray diffraction (XRD) patterns were recorded using a D8-Focus X-ray diffractometer (BRUKER AXS GMBH) equipped with Cu Kα radiation at 40 kV and 40 mA at a scan rate of 8°/min. FT-IR spectra were obtained on a Nicolet 6700 FT-IR spectrometer. Scanning electron microscopy (SEM) images were observed using an APREO field-emission scanning electron microscope. High-resolution transmission electron microscopy (HR-TEM) observations were carried out using a JEM-F200 transmission electron microscope (JEOL) with a field emission gun operating at 200 kV. UV-vis diffuse reflectance spectra (UV-vis DRS) were recorded with a Shimadzu UV-2600 spectrometer equipped with a 60 mm diameter integrating sphere using $BaSO_4$ as the reflectance sample. X-ray photoelectron spectrum (XPS) was conducted to analysis with a K-Alpha+ X-ray photoelectron spectroscope (ThermoFisher Scientific, UK), using Al Kα as the X-ray source. The analyzer's output spectrum was calibrated based upon the binding energy of contaminated C 1*s* (284.80 eV) under vacuum conditions of 5×10^{-8} Pa. The X-ray absorption fine structure spectroscopy (XAFS) was performed by Table XAFS-500A (Anhui Chuangpu Instrument Technology Co., Ltd) equipped with Mo target. The raw XAFS data were preprocessed following the conventional procedure: background removal, normalization, Fourier transformation to k-space, and k^3 weighted EXAFS oscillations. The BET surface area was measured by a Micromeritics ASAP 2020 Automatic Specific Surface Area and Porosity Analyzer. The steady-state photoluminescence (PL) measurement was measured by a FLS1000 (Edinburgh) fluorescence spectrophotometer with the excitation light set at 375 nm. Time resolved fluorescence decay spectra were also measured by the

spectrophotometer at 298 K. Electron spin resonance (ESR) spectra were examined by an electron paramagnetic resonance spectrometer (JES-FA200, JEOL) under visible light irradiation ($\lambda \geq 420$ nm).

Table

Table S1. Specific Surface Area and Pore Volume of Different Samples

Samples	Surface Area m^2/g	Mesopore Volume cm^3/g	Micropore Volume cm^3/g
α-Fe_2O_3	82.18	0.3458	0.03082
PEB-DBT	72.39	0.2465	0.03451
FPD-1	72.91	0.2595	0.04672
FPD-2	63.53	0.1795	0.02996
FPD-3	69.82	0.1816	0.03420

Table S2. Fitting Results of Different Kinetic Models for OFL Degradation

Kinetic Models	Parameter	PEB-DBT	FPD-1	FPD-2	FPD-3
Zero-order	k_0(mg L^{-1} min^{-1})	0.61891	1.63299	1.98976	1.18249
	R^2	0.98997	0.9607	0.97681	0.98509
First-order	k_1(min^{-1})	0.01849	0.08207	0.18786	0.04442
	R^2	0.97973	0.89296	0.85343	0.95274
Second-order	k_2(L/(mg·min))	$5.581*10^{-4}$	0.00507	0.04837	0.00177
	R^2	0.96619	0.83134	0.78177	0.911

Table S3. Fitting Results of Different Kinetic Models for MB Degradation

Kinetic Models	Parameter	PEB-DBT	FPD-2
Zero-order	k_0(mg L^{-1} min^{-1})	3.39239	0.33602
	R^2	0.9573	0.9898
First-order	k_1(min^{-1})	0.02278	0.01182
	R^2	0.99832	0.9822
Second-order	k_2(L/(mmol·min))	0.00119	$4.30754*10^{-4}$
	R^2	0.97586	0.94947

The Zero-order, first-order, and second-order model have been described below[2]:

Zero-order kinetic model:

$$C_0\text{-}C_t = k_0 t$$

First-order kinetic model:

$$\ln (C_t/C_0) = -k_1 t$$

Second-order kinetic model:

$$1/C_t - 1/C_0 = k_2 t$$

C_0 and C_t represent the initial OFL/MB concentration (mg/L) and OFL/MB concentration (mg/L) at sample time t (min), respectively. k_0, k_1, and k_2 are the zero-order, first-order, and second-order kinetic rate constant, respectively.

Figure

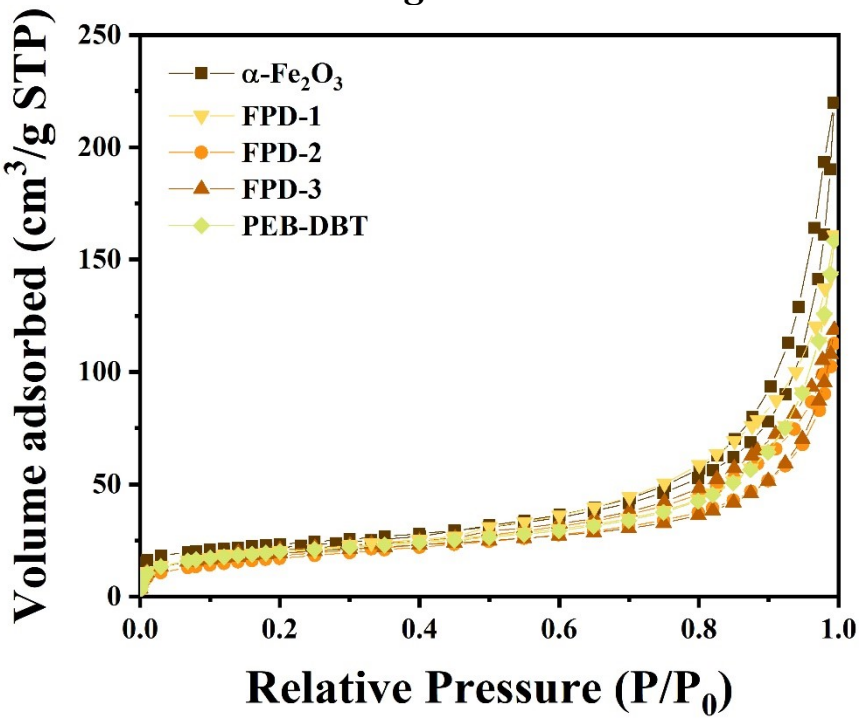

Fig. S1 BET adsorption desorption isotherm of the samples.

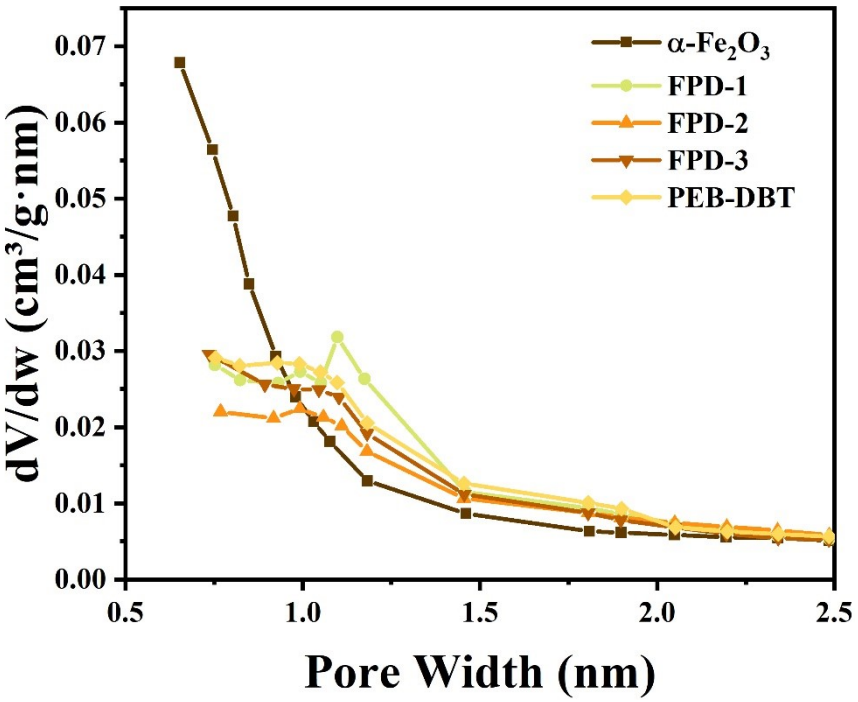

Fig. S2 Micropore distribution of the samples.

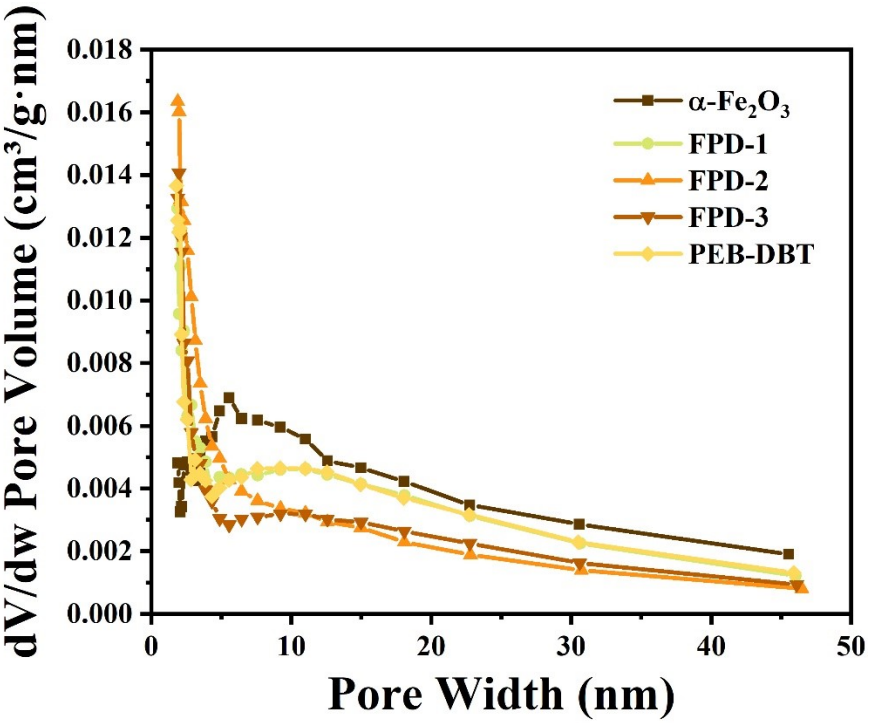

Fig. S3 Mesopores distribution of the samples.

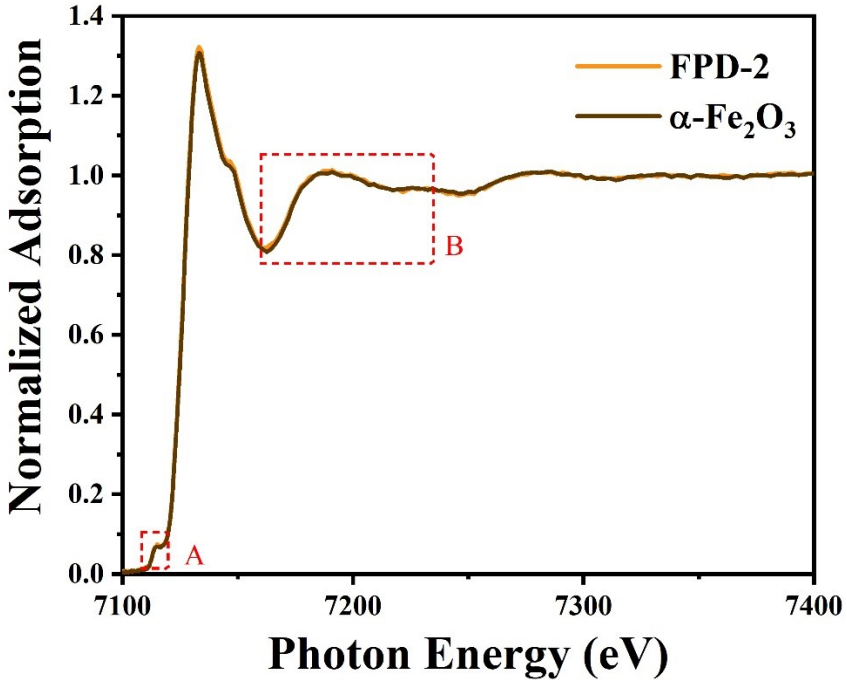

Fig. S4 Fe K-edge XANES spectrum of α-Fe_2O_3 and FPD-2.

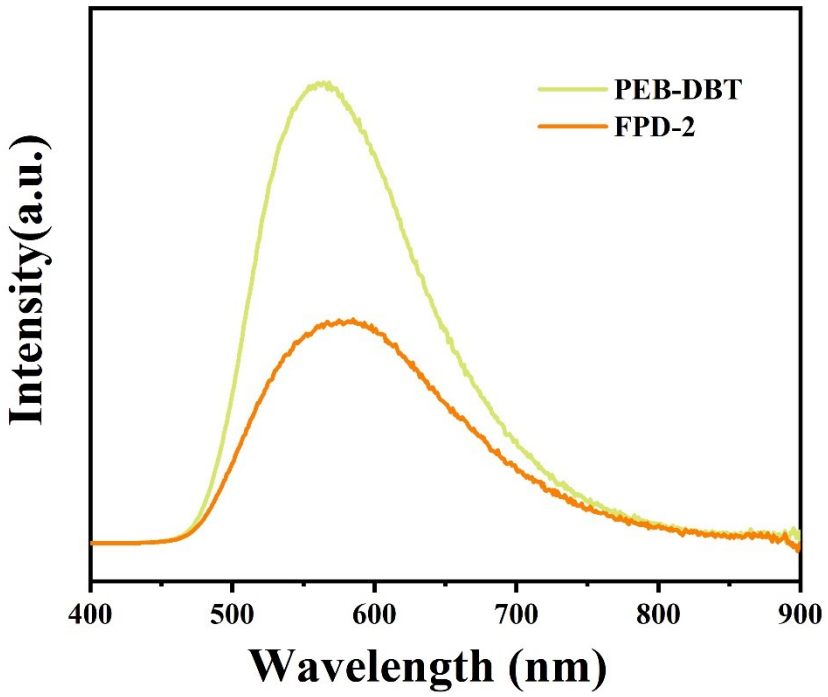

Fig. S5 Steady-state fluorescence intensity spectrum of the samples.

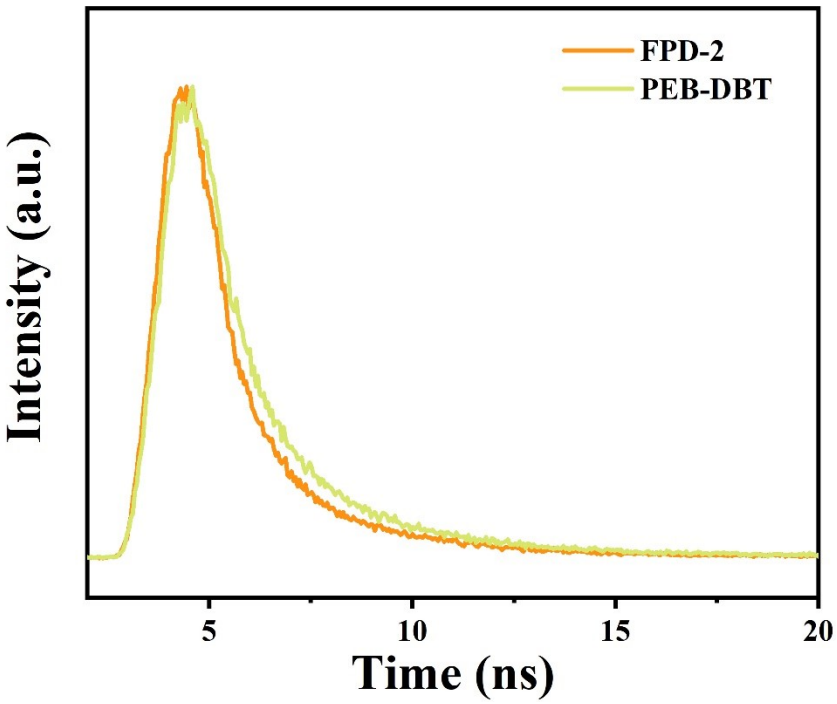

Fig. S6 Transient fluorescence lifetime spectrum of the samples.

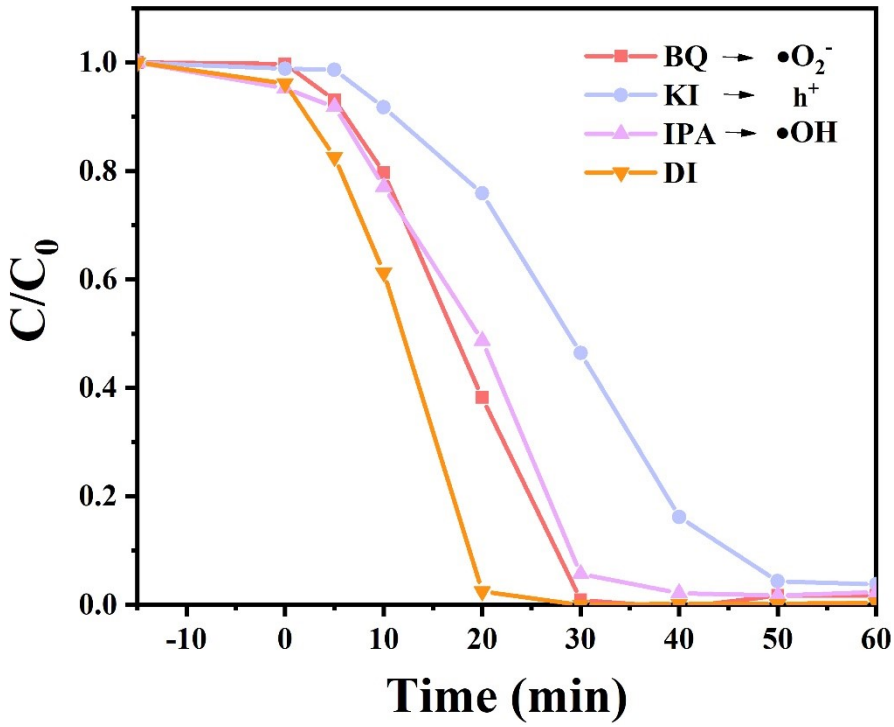

Fig. S7 Scavenger quenching effects on OFL degradation using FPD-2.

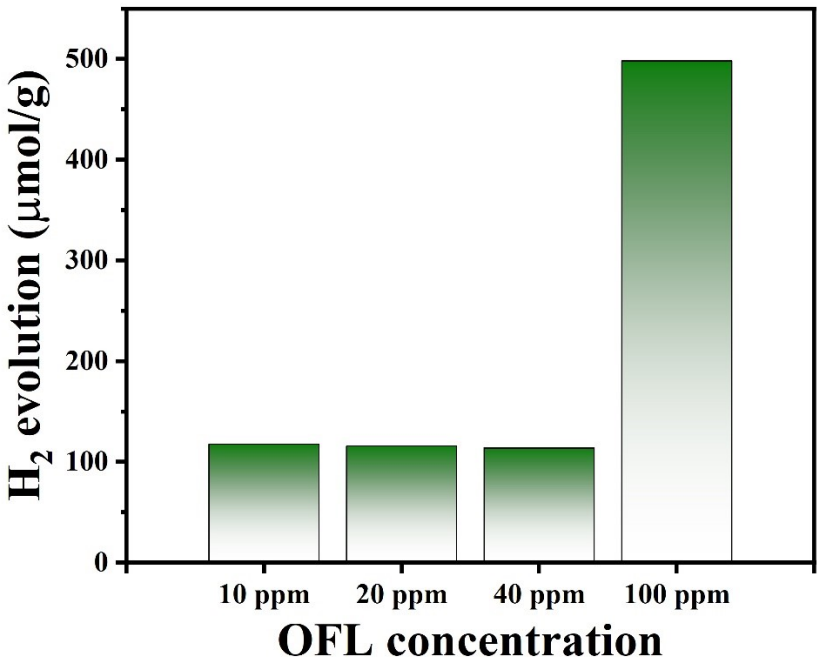

Fig. S8 Hydrogen evolution rate of FPD-2 when degrading OFL with different concentration.

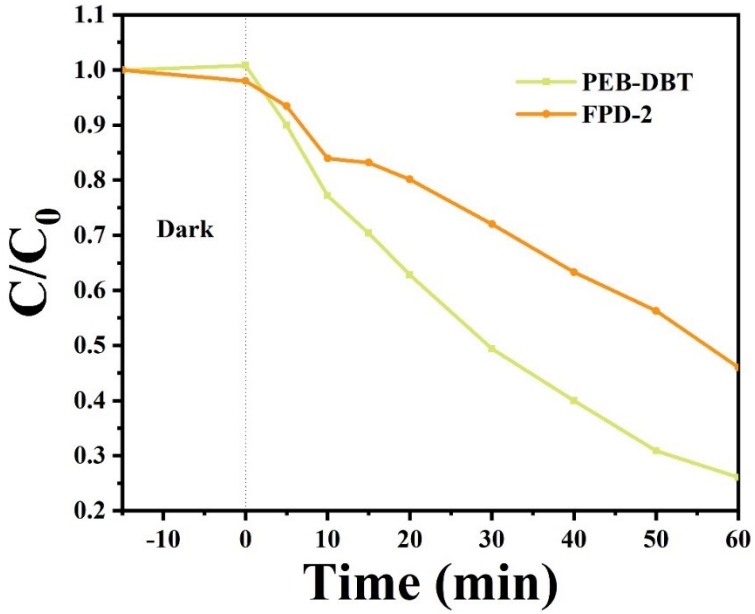

Fig. S9 MB degradation performance of the FPD-2.

The sensitization effect of MB can be ignored in this work. For the MB degradation process with single PEB-DBT, the CB level of MB (-0.25 eV) is more positive than PEB-DBT (-0.83 eV). Therefore, the MB can not act as a dye sensitizer to transfer electrons from MB to PEB-DBT. For the MB degradation process with FPD-2, the CB level of MB (-0.25 eV) is more negative than α-Fe_2O_3 (0.34 eV). Although electrons can transfer from MB to α-Fe_2O_3, the electrons on the CB of α-Fe_2O_3 can not reduce O_2 to form $\cdot O_2^-$ (E_0 = -0.33 V vs. NHE). Thus, the MB degradation performance is suppressed rather than improved by dye sensitizer (**Fig. S9**).

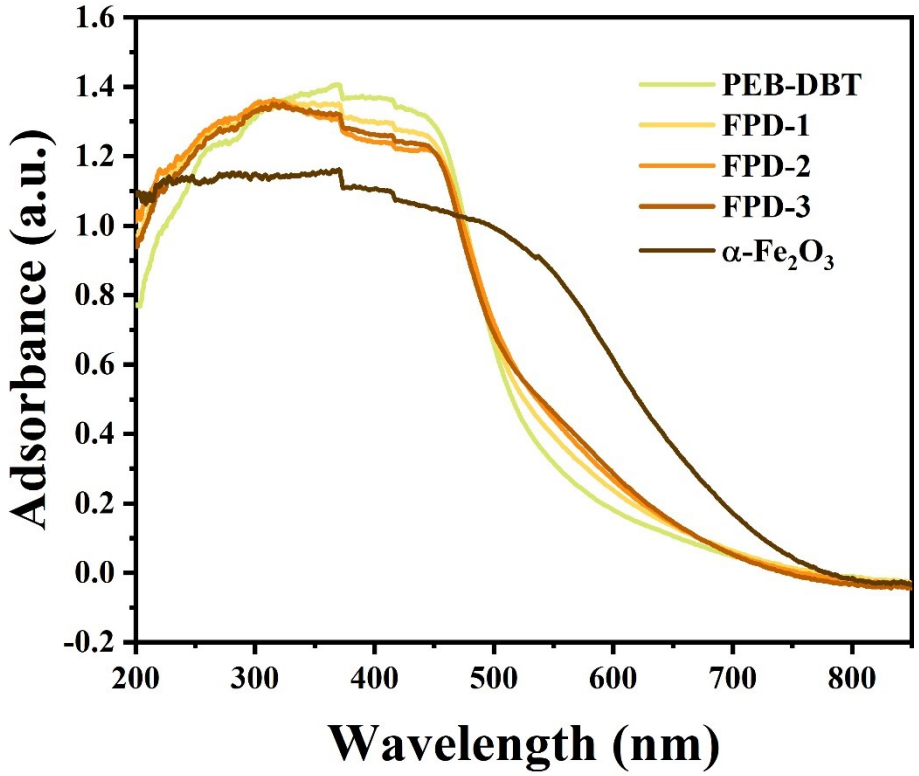

Fig. S10 UV-vis DRS spectra of the samples.

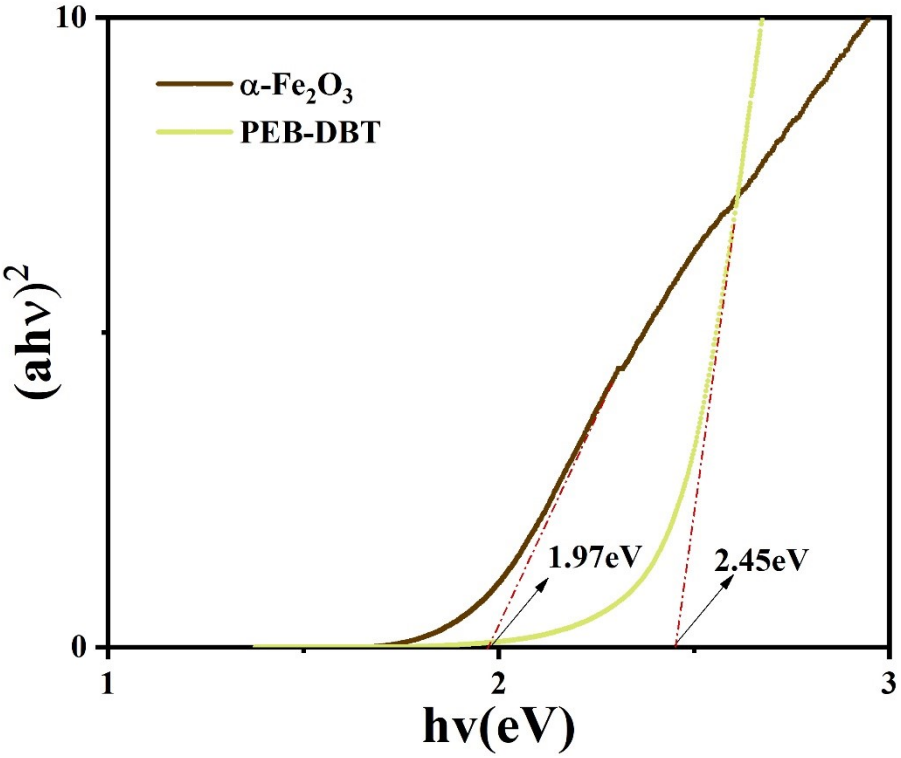

Fig. S11 K-M transformation data of Fe_2O_3 and PEB-DBT.

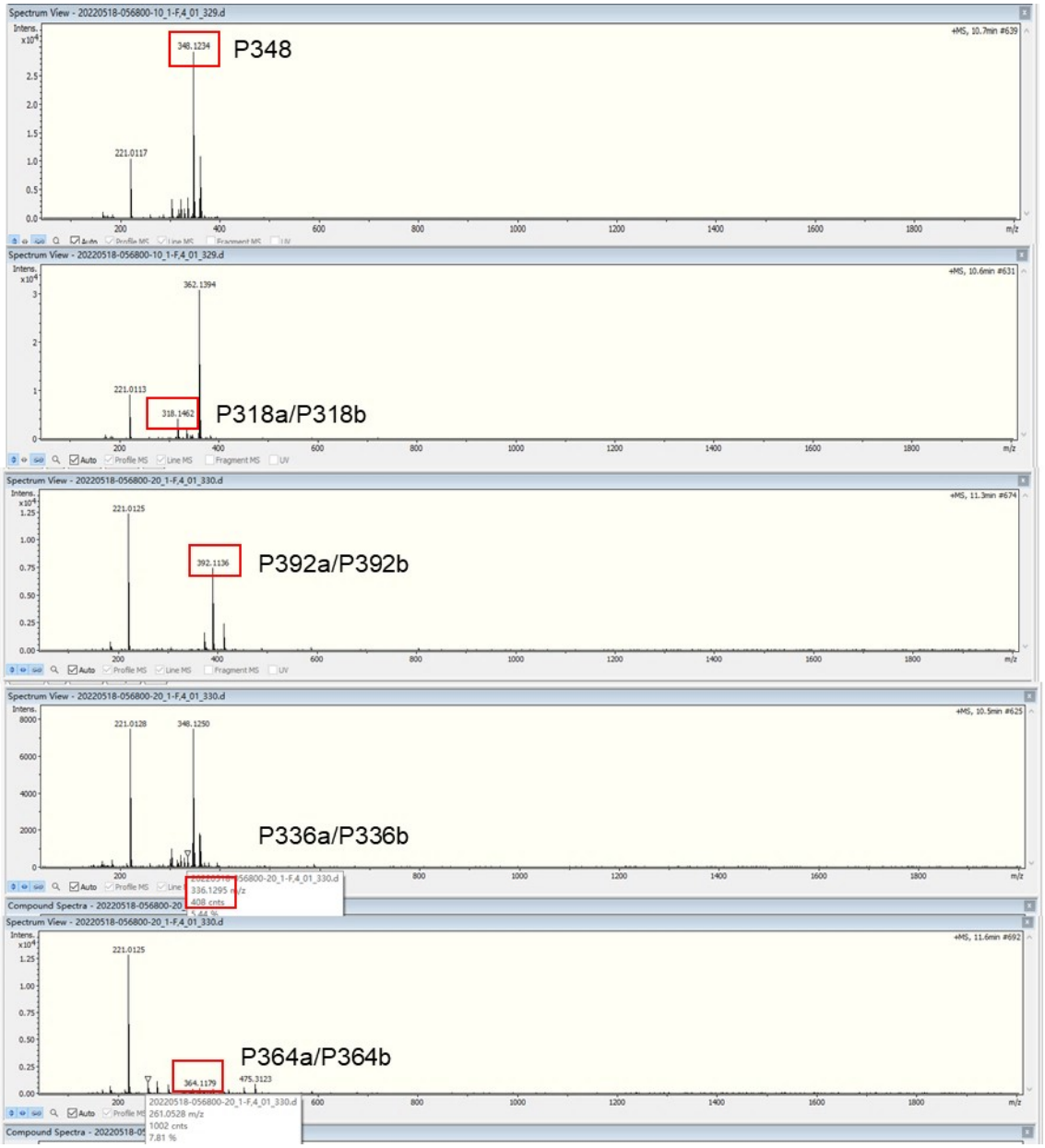

Fig. S12 MS chromatograms for the intermediates (P348, P318a, P318b P392a, P392b, P336a, P336b P364a and P364b) of OFL degradation.

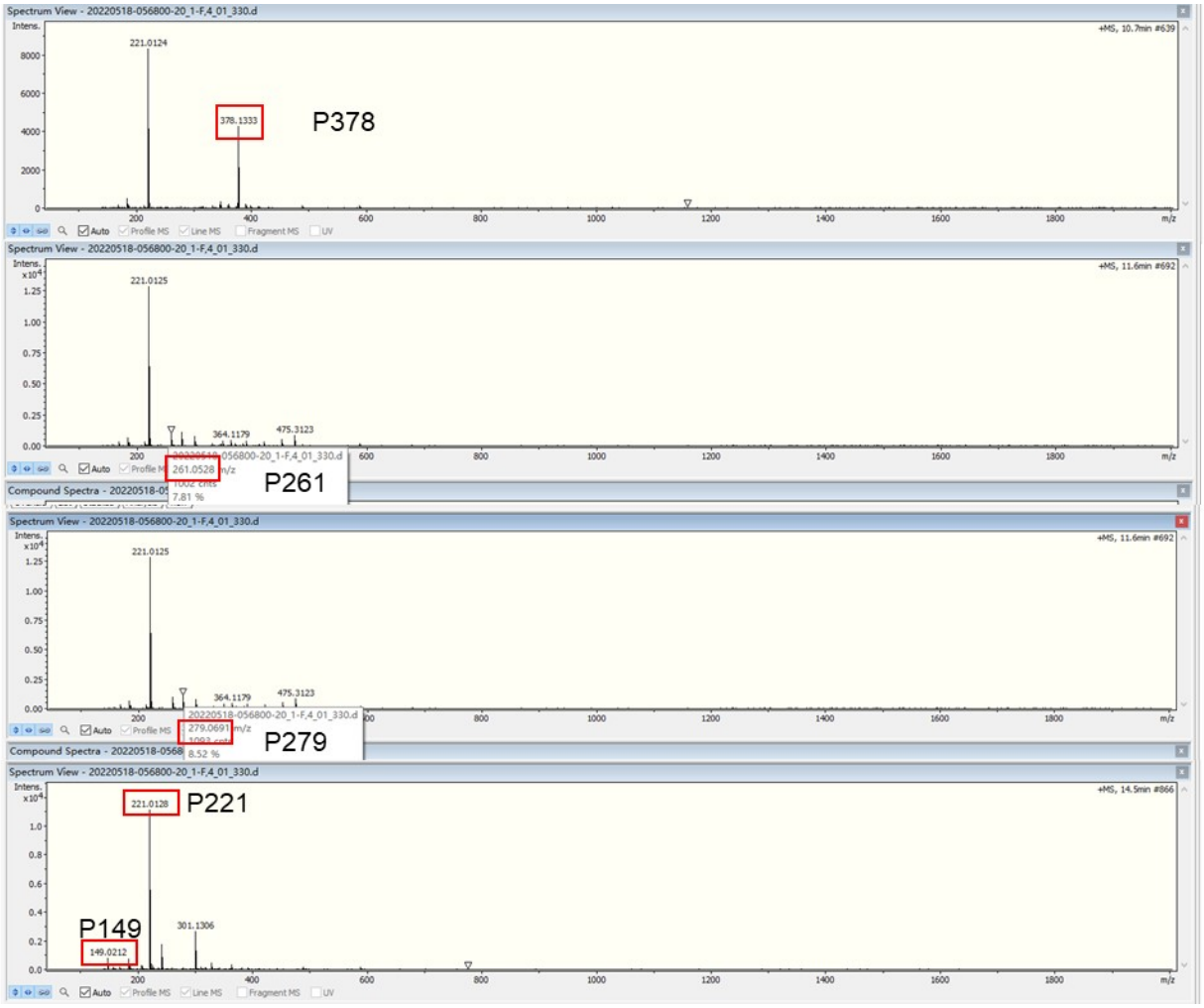

Fig. S13 MS chromatograms for the intermediates (P378, P261, P279 P221 and P149) of OFL degradation.

References

1 M. Sachs, R. S. Sprick, D. Pearce, S. A. J. Hillman, A. Monti, A. A. Y. Guilbert, N. J. Brownbill, S. Dimitrov, X. Shi, F. Blanc, M. A. Zwijnenburg, J. Nelson, J. R. Durrant and A. I. Cooper, *Nat. Commun.* 2018, **9**, 4968.

2 F. Li, T. Huang, F. Sun, L. Chen, P. Li, F. Shao, X. Yang and W. Liu, *Appl. Catal. B.,* 2022, **317**, 121725.

3 Z. Du, K. Li, S. Zhou, X. Liu, Y. Yu, Y. Zhang, Y. He and Y. Zhang, *Chem. Eng. J.,* 2020, **380**, 122427.